Since January 2020 Elsevier has created a COVID-19 resource centre with free information in English and Mandarin on the novel coronavirus COVID-19. The COVID-19 resource centre is hosted on Elsevier Connect, the company's public news and information website.

Elsevier hereby grants permission to make all its COVID-19-related research that is available on the COVID-19 resource centre - including this research content - immediately available in PubMed Central and other publicly funded repositories, such as the WHO COVID database with rights for unrestricted research re-use and analyses in any form or by any means with acknowledgement of the original source. These permissions are granted for free by Elsevier for as long as the COVID-19 resource centre remains active.

Available online at www.sciencedirect.com
ScienceDirect
Virology 367 (2007) 41 – 50
VIROLOGY
www.elsevier.com/locate/yviro

Mutational analysis of a helicase motif-based RNA 5′-triphosphatase/NTPase from bamboo mosaic virus

Yu-Tsung Han, Chia-Sheng Tsai, Ya-Chio Chen, Ming-Kuem Lin, Yau-Heiu Hsu, Menghsiao Meng *

Graduate Institute of Biotechnology, National Chung Hsing University, 250 Kuo-Kuang Rd., Taichung, Taiwan 40227, ROC

Received 31 January 2007; returned to author for revision 6 March 2007; accepted 3 May 2007
Available online 22 June 2007

Abstract

The helicase-like domain of BaMV replicase possesses NTPase and RNA 5′-triphosphatase activities. In this study, mutational effects of the helicase signature motifs and residue L543 on the two activities were investigated. Either activity was inactivated by K643A-S644A, D702A, D730A, R855A, or L543P mutations. On the other hand, Q826A, D858A and L543A had activities, in terms of k_{cat}/K_m, reduced by 5- to 15-fold. AMPPNP, a nonhydrolyzable ATP analogue, competitively inhibited RNA 5′-triphosphatase activity. Analogies of mutational effects on the two activities and approximation of $K_{i(AMPPNP)}$ and $K_{m(ATP)}$ suggest that the catalytic sites of the activities are overlapped. Mutational effects on the viral accumulation in *Chenopodium quinoa* indicated that the activities manifested by the domain are required for BaMV survival. Results also suggest that Q826 in motif V plays an additional role in preventing tight binding to ATP, which would otherwise decrease further RNA 5′-triphosphatase, leading to demise of the virus in plant.
© 2007 Elsevier Inc. All rights reserved.

Keywords: RNA 5′-triphosphatase; NTPase; ATPase; Helicase-like protein; Bamboo mosaic virus, Potexvirus; Alphavirus-like superfamily

Introduction

Bamboo mosaic virus (BaMV), a member of potexvirus genus belonging to the alphavirus-like superfamily, has a positive-strand RNA genome (~6.4 kb) with a 5′ m^7GpppG cap structure and a 3′ poly(A) tail (Lin et al., 1994). Open reading frame 1 of the viral genome encodes a 155-kDa replicase consisting of mRNA capping enzyme, helicase-like and RNA-dependent RNA polymerase (RdRp) domains sequentially from N to C termini. A disordered region of more than 100 amino acid residues and a proline-rich segment separate respectively the neighboring functional domains. These two flexible regions may allow one domain to interact with others dynamically during the viral replication process. The capping enzyme domain, expressed in membrane fractions of yeast, exhibited an *S*-adenosylmethionine-dependent guanylyltransferase activity by which GTP is methylated to form m^7GTP before the m^7GMP moiety is further transferred to the 5′-diphosphate end of mRNA to form the m^7GpppN cap structure (Huang et al., 2005; Li et al., 2001a). Such distinctive capping activity has also been demonstrated in Semliki Forest virus (SFV) (Ahola and Kääriäinen, 1995), brome mosaic virus (Ahola and Ahlquist, 1999; Kong et al., 1999), tobacco mosaic virus (TMV) (Merits et al., 1999) and hepatitis E virus (Magden et al., 2001); thus, it is probably a common feature of the capping enzymes from the alphavirus-like superfamily. The *E. coli*-expressed helicase-like domain possessed both RNA 5′-triphosphatase and NTP hydrolase activities (Li et al., 2001b). With the RNA 5′-triphosphatase and the aforementioned capping enzyme activities, a cap structure could be formed at the 5′ end of BaMV mRNA *in vitro*. The recombinant RdRp domain showed a template-dependent RNA polymerase activity and had preferential binding activity to the 3′ noncoding region of the viral RNA (Huang et al., 2001; Li et al., 1998).

RNA 5′-triphosphatase specifically cleaves the 5′ γ-phosphate out of the nascent mRNA in the first reaction step toward the cap formation. The documented RNA 5′-triphosphatases can be grouped into three classes according to their primary structures and the catalytic mechanism employed. The meta-

* Corresponding author. Fax: +886 4 22853527.
E-mail address: mhmeng@dragon.nchu.edu.tw (M. Meng).

0042-6822/$ - see front matter © 2007 Elsevier Inc. All rights reserved.
doi:10.1016/j.virol.2007.05.013

zoan and plant enzymes are of the metal-independent cysteine phosphatase type and distinguish themselves by possessing an $HC(X)_5RS/T$ motif, in which the cysteine residue acts as a catalytic nucleophile within the catalytic pathway (Changela et al., 2001; Takagi et al., 1997). The enzymes from fungi, protozoa, and some DNA viruses constitute a metal-dependent phosphohydrolases class with characteristic of possessing two essential glutamate-containing motifs (Ho et al., 1998; Martins and Shuman, 2003). RNA triphosphatases, derived from RNA helicases or helicase-like proteins, constitute another metal-dependent phosphohydrolases class. This class includes the enzymes identified from RNA viruses such as reovirus (Bisaillon and Lemay, 1997; Bisaillon et al., 1997), alphavirus (Vasiljeva et al., 2000), dengue virus (Matusan et al., 2001), coronavirus (Ivanov et al., 2004; Ivanov and Ziebuhr, 2004), and BaMV (Li et al., 2001b). Both classes of the metal-dependent RNA triphosphatases are also capable of hydrolyzing nucleoside triphosphates to nucleoside diphosphates and inorganic phosphate.

According to motif-based classification, helicase-like proteins from RNA viruses have been classified into three superfamilies (SF) (Kadaré and Haenni, 1997). Members of SF1 share similarity to nsp2 of alphavirus, while NS3-like proteins of potyvirus, flavivirus and pestivirus, and 2C-like proteins of picornavirus are representatives of SF2 and SF3, respectively. Across the three SF, GKS/T sequence of motif I (Walker A site) is conserved, whereas the consensus sequences of motif II (Walker B site) are varied, with DE/D sequences in SF1 and SF3 and DEXH in SF2. Based on the classification principle, the helicase-like domain of BaMV replicase can be grouped into SF1. Fig. 1 shows comparison of partial amino acid sequences of the BaMV domain and some of the SF1 members. In relation to enzymatic activities, all three SF proteins have ATPase activity. An RNA helicase activity has also been broadly corroborated on proteins of SF2; however, the activity was so far demonstrated only on a couple of SF1 proteins, e.g., nsp2 of SFV (Gomez de Cedron et al., 1999) and the helicase domain of TMV replicase (Goregaoker and Culver, 2003). Like the helicase-like domain of BaMV replicase, nsp2 of SFV has also been reported to have RNA 5′-triphosphatase activity (Vasiljeva et al., 2000).

NTP binding and hydrolysis functions of motif I and II of helicases have been suggested by numerous mutational studies and confirmed by crystal structures of helicases such as PcrA of *Bacillus stearothermophilus* (Subramanya et al., 1996; Velankar et al., 1999), Rep of *Escherichia coli* (Korolev et al., 1997) and NS3 of hepatitis C virus (Yao et al., 1997). The lysine residue of motif I interacts with the phosphates of MgATP/MgADP and the threonine or serine ligates the Mg^{2+} ion. The first aspartic acid of motif II also coordinates Mg^{2+} ion and the following glutamate or aspartate residue may act as catalytic base in ATP hydrolysis. By contrast, functions of other signature motifs, particularly those of SF1, are relatively less addressed. As a step toward better understanding the relationship between activities and structures of the helicase-like domain of BaMV replicase, we set out to investigate the importance of each signature motif to its NTPase and RNA 5′-triphosphatase activities by mutational and kinetic analyses. Results of this study strongly suggest a common catalytic site for the removal of 5′γ-phosphate from NTP and RNA. The relation between the enzymatic activities *in vitro* and the viral replication *in vivo* is also discussed in this study.

Results

Mutations

Previous studies demonstrated that the helicase-like domain of BaMV replicase exhibits an Mg^{2+}/Mn^{2+}-dependent γ-phosphohydrolase activity toward both nucleoside triphosphate and RNA (Li et al., 2001b). The former (NTPase) could be a prerequisite for the putative RNA helicase activity, and the latter (RNA 5′-triphosphatase) could be involved in the cap structure formation. Substitution of GAA for GKS in motif I abolished NTPase as well as RNA 5′-triphosphatase activities. In the present study, we examined the mutational effects of other conserved motifs of SF1 helicases with respect to these two activities. Leucine at position 543 was also included in the mutation list because the accumulation level of the viral coat protein decreased significantly in protoplast of *Nicotiana benthamiana* as Leu543 to proline mutation was introduced into the viral replicase (Huang and Tsai, 1998). In addition, a DEIH sequence immediately downstream motif VI was mutated because it is analogous to DEXH box of motif II of SF2. Each of the targeted residues, as indicated in Fig. 1, was replaced by alanine except Leu543 that was also replaced by proline. All the proteins were expressed in *E. coli* and purified by immobilized metal affinity and anionic exchange chromatography as described in Materials and methods. The purification results are shown in Fig. 2.

Mutational effects on NTPase

The importance of the mutated residues to ATP hydrolysis activity was first analyzed qualitatively by TLC assay (Fig. 3). Alanine substitution at K643-S644 or at D702 reduced the activity to extents similar to the background level. Mutation of D730 or R855 to alanine or L543 to proline also resulted in severe damage to ATP hydrolysis activity. In contrast, Q826A and D858A remained active but with diminished activities. ATPase activity manifested by helicases of SF2, e.g., NS3 proteins of yellow fever virus (Warrener et al., 1993), hepatitis C virus (Suzich et al., 1993) and bovine viral diarrhea pestivirus (Tamura et al., 1993), is usually stimulated by single stranded RNA. Effect of RNA on ATPase activity of the BaMV helicase-like domain was also examined in this study. Inclusion of an RNA transcript, corresponding to the first 200 nucleotides of BaMV genome, in the reactions did not cause apparent changes in the ATPase activity of any of the tested enzymes.

To better characterize the NTPase activity, steady-state rates of the reaction were measured by enzyme-coupled assay, in which NTP hydrolysis was coupled to NADH oxidation. Apparent K_m and k_{cat} of the wild-type enzyme toward four different mononucleotides were subsequently calculated based on NTP concentration dependences of rate (Table 1). All four

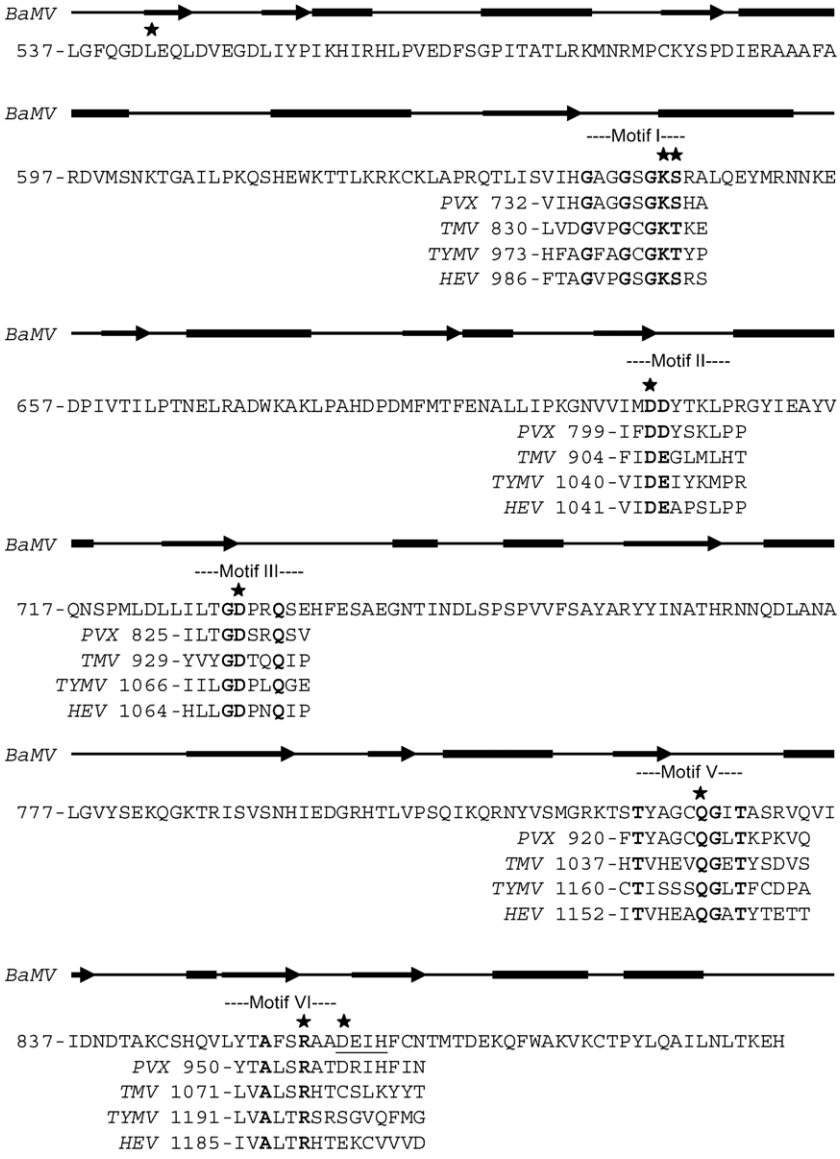

Fig. 1. Alignment of partial amino acid sequences of the helicase-like domains of some RNA viral replicases. The consensus residues within each signature motif of SF1 helicases are shown in bold. Residues mutated in this study on BaMV protein are indicated by asterisk. Protein secondary structure was predicted at the PSIPRED Protein Structure Prediction Server (http://bioinf.cs.ucl.ac.uk/psipred/). The rectangle and arrow symbolize the α-helix and β-strand, respectively. BaMV, PVX, TMV, TYMV, and HEV represent bamboo mosaic virus, potato virus X, tobacco mosaic virus, turnip yellow mosaic virus and hepatitis E virus, respectively.

mononucleotides could be hydrolyzed by the wild-type enzyme at rates with apparent K_m value ranging from 0.15 to 0.33 mM and apparent k_{cat} from 24 to 67 s^{-1}. The specificity constants (k_{cat}/K_m) of the reactions are comparable to that of λ1 of reovirus and nsp13 of SARS coronavirus (Bisaillon et al., 1997; Ivanov et al., 2004) and larger than that of nsp2 of SFV and NS3 of dengue virus (Matusan et al., 2001; Vasiljeva et al., 2000). Mutational effects of the targeted amino acid residues on the apparent kinetic parameters of ATPase were subsequently analyzed by enzyme-coupled assays. Consistent with TLC results, proteins with specified mutation in motif I, II, III or VI did not show ATPase activity to any appreciable extent (not shown). L543P mutant was also inactive; however, L543A was active with an unchanged K_m but a 14-fold reduced k_{cat} (Table 2). D858A had K_m and k_{cat} reduced by factors of 2 and 10, respectively. Q826A had 17-fold and 90-fold decreases in values of K_m and k_{cat}, respectively. It is worth noting that the specificity constant of Q826A decreased only by a factor of 5.3; this and overtime incubation may account for the apparent ATPase activity of Q826A shown in the previous TLC assay. The significantly enhanced affinity to ATP should account for, to some extent, the dramatic decrease of k_{cat} in Q826A.

Mutational effects on RNA 5′-triphosphatase

Besides NTPase activity, the helicase-like domain of BaMV replicase also catalyzes the removal of 5′ γ-phosphate from triphosphate-terminated RNA. Results of typical experiments with wild-type enzyme are shown in Fig. 4. Phosphate increased steadily with time in the first 5 min under the reaction condition

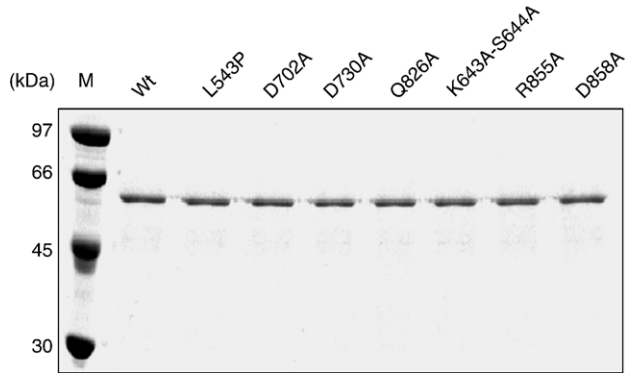

Fig. 2. Protein purification of the helicase-like domain of BaMV replicase. The *E. coli*-expressed enzymes were purified through immobilized metal affinity and anionic exchange chromatography as described under Materials and methods. Each of the purified enzymes was resolved on SDS–PAGE (10%) and stained by Coomassie blue.

(panel A). In addition, phosphates released were roughly proportional to the applied amounts of enzyme within a short period of reaction time (panel B). To define the mutational effects on the activity, reactions catalyzed by wild-type and various mutants were allowed to occur under conditions of enzyme excess (Fig. 5). The activities of K643A-S644A and D702A were nearly abolished. Likewise, L543P, D730A and R855A had activities hardly to be observed. The apparent activity of L543A was comparable to that of wild type, while that of Q826A and D858A was reduced noticeably. To characterize the effects in detail, reaction rates of L543A, Q826A, D858A and the wild-type enzyme were determined at different RNA concentrations, and the kinetic parameters were subsequently calculated (Table 2). Considering the limitations, such as suboptimal substrate concentration, in data processing, the determined values of K_m and k_{cat} were apparent. Still, they should be helpful to evaluate the mutational effects. Comparing with mononucleotides, RNA was hydrolyzed at much slower rates. Alanine substitution at L543, Q826 or D858 had unfavorable effects on both RNA binding and catalysis as evidenced by the increase of apparent K_m and the decrease of apparent

Table 1
Kinetic parameters of NTP hydrolysis catalyzed by wild-type helicase-like domain of BaMV replicase

Substrate	K_m (μM)	k_{cat} (s^{-1})	k_{cat}/K_m (μM^{-1} s^{-1})
ATP	150	67	0.45
GTP	210	35	0.17
UTP	220	24	0.11
CTP	330	30	0.09

The enzymatic activity was determined at 20 °C by enzyme-coupled assay in 1 ml solution that contained 10 pmol enzyme, 0.1 to 3 mM NTP and other buffer components as described under Materials and methods except that the amounts of pyruvate kinase were increased up to 50, 75 and 300 U for GTPase, UTPase and CTPase assay, respectively, to assure the rate of NTP hydrolysis being the limiting step within the coupling reaction.

k_{cat}, respectively. In general, the specificity constants of the three mutants for RNA hydrolysis reduced approximately 5- to 14-fold.

Competitive inhibition of AMPPNP on RNA 5′-triphosphatase

Overall, effects of the investigated mutations on ATPase and RNA 5′-triphosphatase were parallel, implying that the catalytic sites of the two activities are overlapped. To support the notion, effects of AMPPNP, a nonhydrolyzable analogue of ATP, and AMP on RNA 5′-triphosphatase activity were examined. AMPPNP exerted an inhibitory effect on the activity (Fig. 6A). The higher concentration of AMPPNP, the greater extent of inhibition was observed. By contrast, AMP did not significantly affect RNA 5′-triphosphatase activity even as its concentration was up to 2 mM (Fig. 6B), suggesting that the 5′-terminal γ- and β-phosphate groups of substrates are the major determinants for the competition. To know the inhibition mode of AMPPNP, the dependence of rate on RNA substrate concentration was determined under different AMPPNP concentration (Fig. 7A). Double-reciprocal plot of the data showed an approximately unchanged V_{max} (Fig. 7B), suggesting that AMPPNP acted as a competitive inhibitor. The apparent K_i value of AMPPNP in inhibiting RNA 5′-triphosphatase activity

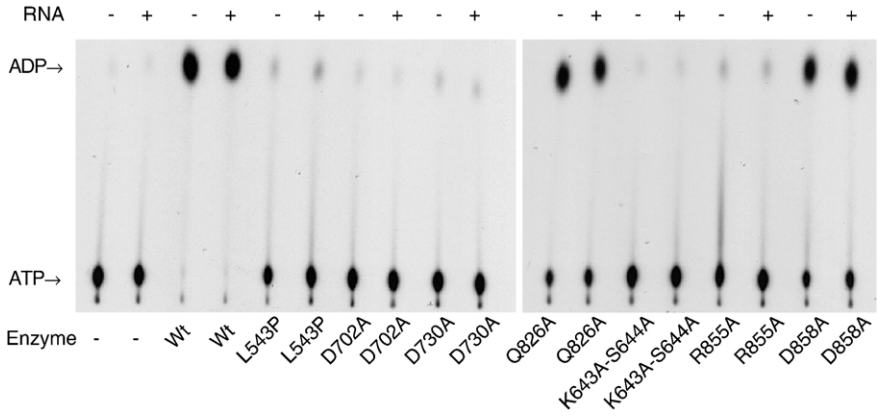

Fig. 3. Analysis of ATPase activities of the wild-type and mutant helicase-like domains of BaMV replicase by TLC. The activity assay was carried out for 20 min in 10 μl solution that contained basically 20 μM ATP, 5 μCi [α-^{32}P] ATP (6000 Ci/mmol, PerkinElmer) and 1 pmol purified protein. Presence or absence of 0.16 μM RNA (200 nt) was as indicated. The reaction products were analyzed by PEI TLC and autoradiography.

Table 2
Effects of selected mutations on ATPase and RNA 5′-triphosphatase activities

Enzyme [a]	ATPase [b]		RNA 5′-triphosphatase [c]	
	K_m (μM)	k_{cat} (s^{-1})	K_m (μM)	k_{cat} (min^{-1})
Wt	150±35	67±15	59±17	4.5±0.9
L543A	150±45	4.6±0.6	82±23	1.2±0.2
Q826A	8.7±2.3	0.73±0.07	120±34	1.0±0.4
D858A	73±26	6.2±0.7	220±50	1.2±0.4

[a] Results of L543P, D702A, D730A, R855A and K643A-S644A are omitted because their activities were undetectable under the reaction conditions.

[b] ATPase activity was determined at 20 °C by enzyme-coupled assay in 1-ml solution that contained 0.1 to 3 mM ATP, 10 to 600 pmol enzyme and other buffer components as described under Materials and methods. Data are averages of at least two independent experiments.

[c] RNA 5′-triphosphatase activity was determined by TLC analysis. Reactions were carried out at 20 °C in 3-μl solution that contained 1 pmol enzyme, 10 to 80 μM 5′-[γ-^{32}P]RNA, and other buffer components as described under Materials and methods. Data are averages of two independent experiments.

was calculated to be 93 μM, which is comparable to the K_m value of ATP. Probably, the catalytic sites for hydrolyzing 5′ γ-phosphate from RNA and mononucleotide are identical or extensively overlapped.

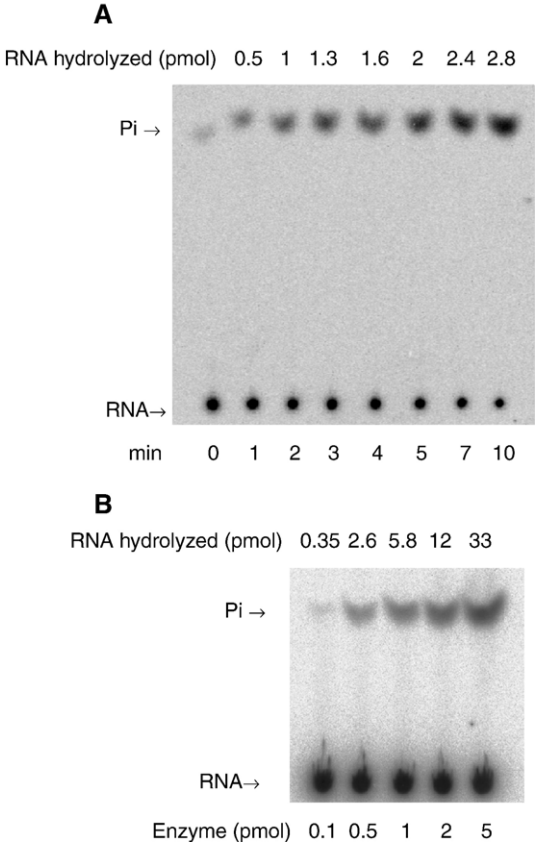

Fig. 4. RNA 5′-triphosphatase reaction catalyzed by the wild-type enzyme. (A) Time course of reactions in 5 μl solution that contained 0.1 pmol purified protein, 1 μM 5′-[γ-^{32}P]RNA and other components as described under Materials and methods. (B) Reactions carried out for 1 min in 3 μl solution that contained 240 pmol (80 μM) 5′-[γ-^{32}P]RNA, indicated amounts of enzyme and other components as described under Materials and methods.

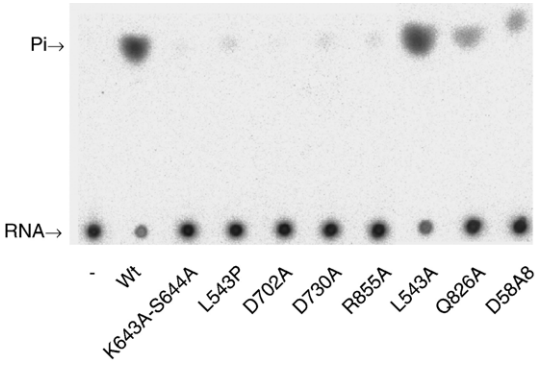

Fig. 5. Analysis of RNA 5′-triphosphatase activity of the wild-type and mutant helicase-like domains of BaMV replicase by TLC. The activity assay was carried out for 40 min in 3 μl solution that contained 1.4 μM 5′-[γ-^{32}P]RNA, 10 pmol purified protein and other components as described under Materials and methods.

Mutational effects on the viral accumulation in plant

The competence of BaMV to multiply *in vivo* was investigated by inoculating plasmid pCBG into leaves of *C. quinoa*, in which the viral replication and cell-to-cell movement could

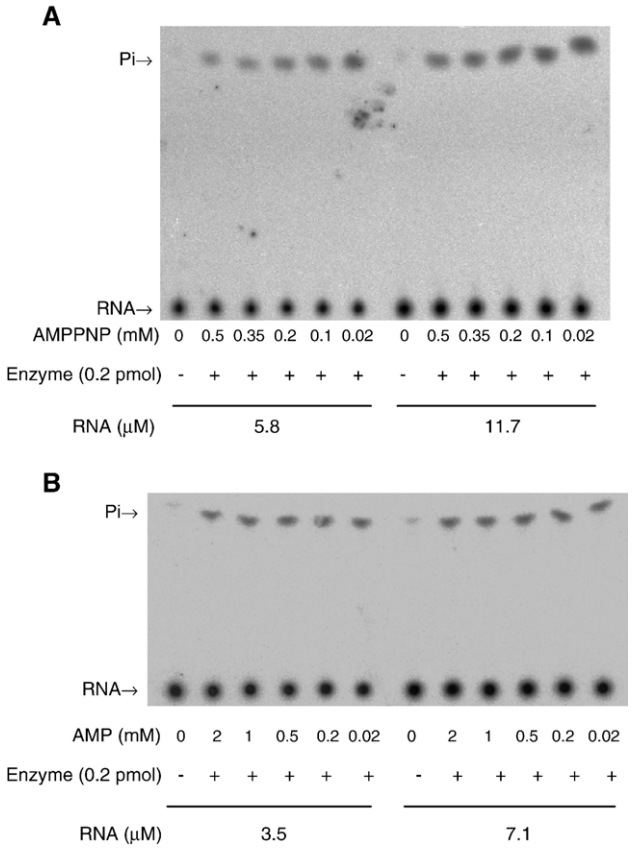

Fig. 6. Inhibition of RNA 5′-triphosphatase activity by AMPPNP and AMP. (A) Reactions were carried out for 1 min in 5 μl solution that contained 5.8 or 11.7 μM 5′-[γ-^{32}P]RNA, 0.25 pmol purified protein, indicated amounts of AMPPNP, and other components as described under Materials and methods. Reaction products were detected by TLC. (B) Reactions were carried out in the presence of indicated concentration of AMP under similar conditions as described in panel A.

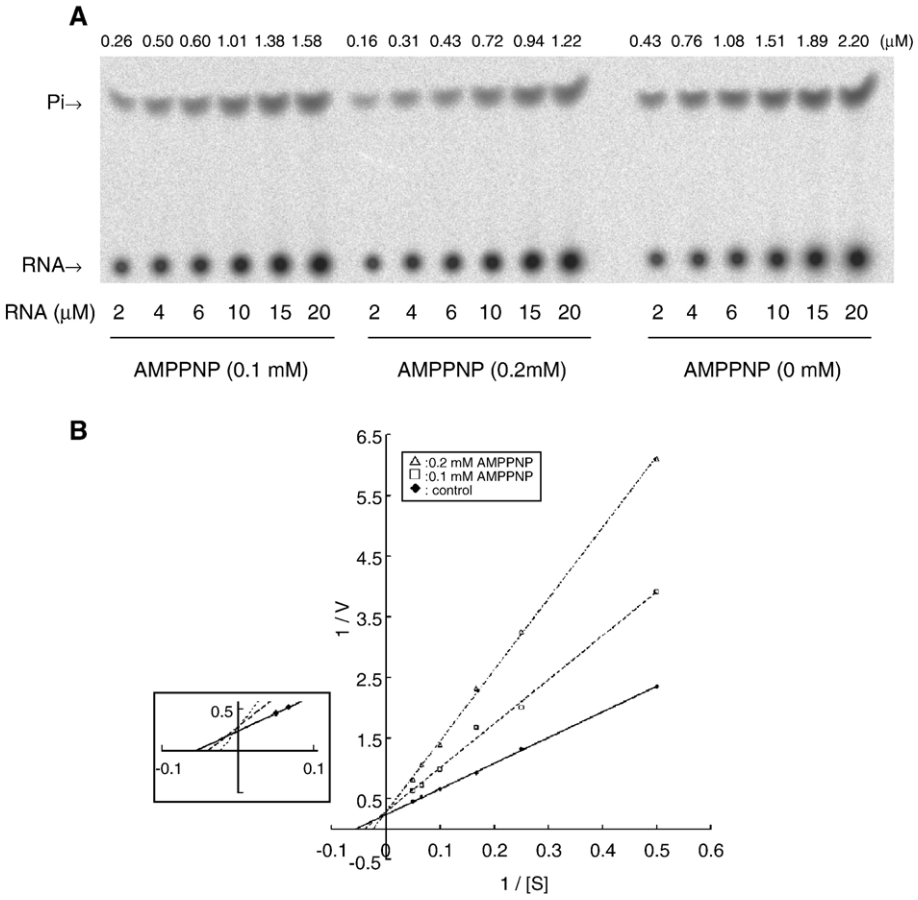

Fig. 7. Competitive inhibition of RNA 5′-triphosphatase activity by AMPPNP. (A) One minute reactions were preformed in 3 μl solution containing 3 pmol purified protein, indicated concentrations of RNA and AMPPNP, and other components as described under Materials and methods. (B) Lineweaver–Burk plot of the results of panel A. The scales of *X*- and *Y*-axes are in μM^{-1} and min, respectively.

be monitored by the appearance of green fluorescence because the expression of the introduced GFP depends on the fulfillment of BaMV replication (Lin et al., 2004). To see the mutational effects, each of the selected mutations was introduced into pCBG, and the resulting mutant plasmid was mechanically inoculated into plant cells. As shown in Fig. 8, spots with green fluorescence began to appear on leaves of plants infected with wild type, L543A, or D858A virus a week later after inoculation. The respective frequency and average diameter of fluorescent loci appeared on leaves were similar, suggesting that the three variants replicated equally well in *C. quinoa*. Local lesions formed later on leaves that had shown green fluorescence spots earlier (Fig. 9). No signs of green fluorescence or disease symptoms were noted on leaves of plants infected with other mutant viruses, including that carries Q826A mutation. Repeated experiments with wild type, L543A, Q826A and D858A confirmed the negative result of Q826A mutation. Disability on RNA 5′-triphosphatase alone is sufficient to account for the replication incompetence of those carrying specified mutation in motif I, II, III, and VI and L543P since formation of 5′ cap at viral mRNA is essential for substantial viral protein translation. However, the reasons for the opposite effects of the D858A and Q826A mutations in plant are uncertain because the two mutations decreased RNA 5′-triphosphatase activity to similar extents. Would it be possible that alanine substitution at Q826 affects not only the enzymatic activity but also the protein stability? Protein stabilities of wild type, L543A, Q826A and D858A were, therefore, investigated under 25 °C by measuring their residual enzymatic activity as a function of time. The inactivation of the proteins followed first-order kinetics. The half lives ($t_{1/2}$) of wild type, L543A and Q826A were approximately 2 h, whereas $t_{1/2}$ of D858A was 40 min (data not shown), indicating that protein stability would not be the cause. Alternatively, the distinct feature of Q826A on ATPase activity might underlie the failure of the mutant virus to replicate *in vivo*. The mutant protein might not be capable of providing sufficient energy by hydrolyzing ATP to the putative helicase activity, or the tight binding of ATP deteriorated further the weakened RNA 5′-triphosphatase activity. Activity of RNA 5′-triphosphatase was assayed in the presence of 0.3 mM ATP, which is within physiological concentration range (Hampp et al., 1982; Usuda, 1988), to explore the latter possibility (Fig. 10). Under the competition conditions, RNA 5′-triphosphatase activities of wild type and D858A remained approximately 30%, whereas little was left in Q826A mutant. The results suggest that RNA and mononucleoside triphosphate could have reciprocal inhibitory effects *in vivo*; and the

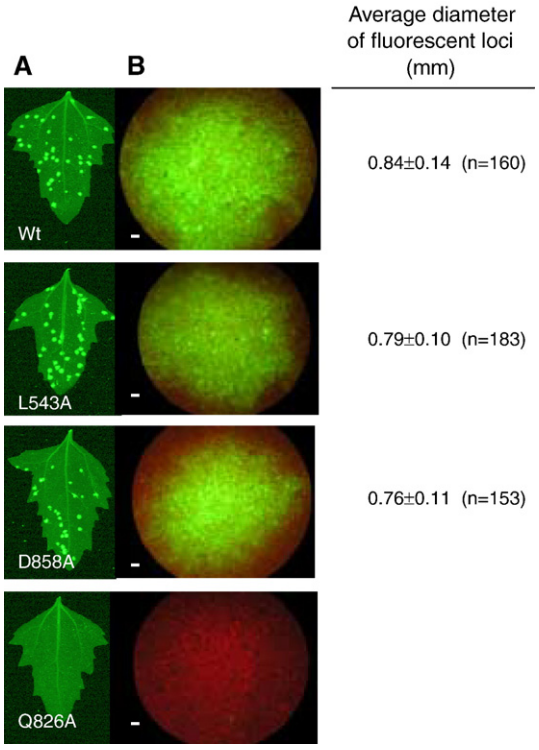

Fig. 8. Fluorescent images of the leaves of *C. quinoa* at the 7th day post inoculation with wild-type and mutant BaMV clones. Inoculation of *C. quinoa* leaves with pCBG, a recombinant BaMV infectious clone, and its mutants was as described under Materials and methods. (A) Observation of entire infected leaves with FluorImager. (B) Spread of green fluorescence protein within a single focus under fluorescent microscope. The white scale bar represents 50 μm. Results from inoculation of mutant pCBG harboring L543P, D702A, D730A, R855A or K643A-S644A were identical to that of Q826A and are omitted.

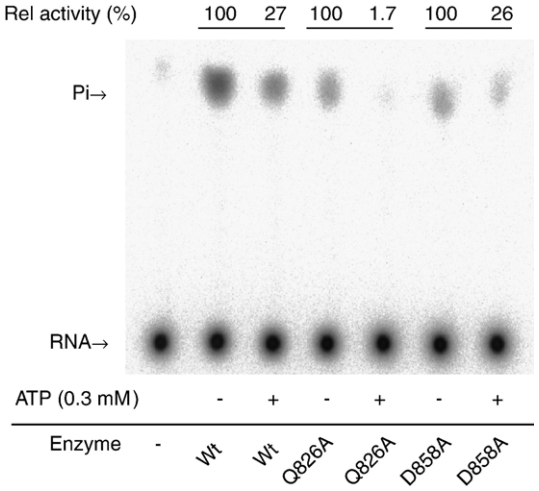

Fig. 10. Inhibition of RNA 5′-triphosphatase by ATP. Reactions were carried out for 5 min in 5 μl solution that contained 10 μM 5′-[γ-^{32}P]RNA, 0.3 mM ATP, wild-type enzyme (1.2 pmol) or mutant enzymes (each 10 pmol) and other components as described under Materials and methods. For each enzyme, activity in the presence of ATP is reported relative to activity in the absence of ATP.

deterioration of RNA 5′-triphosphatase activity might be simply enough to disable the replication function of Q826A mutant virus.

Discussion

Helicases are defined as proteins that catalyze the separation of duplex nucleic acids into single strands in an NTP-dependent reaction. Sequence comparison of the helicase-like proteins from RNA viruses has disclosed the conservation of several signature motifs and grouped them into three SF (Kadaré and Haenni, 1997). Functions of helicase motifs have been addressed through mutational and structural analyses owing to the involvement of helicases in various important biological processes. As regards SF1, crystal structures of DNA helicases PcrA (Subramanya et al., 1996; Velankar et al., 1999) and Rep (Korolev et al., 1997) could provide us insights into the relationships between structures and functions of the proteins. In brief, residues on both motif I and II are involved in the binding of ATP through phosphate group recognition and Mg^{2+} coordination, while the second conserved acidic residue of motif II acts as catalytic base in ATP hydrolysis. Other residues such as the glutamine of motif III and the arginine of motif VI also participate in accommodating the γ-phosphate group of ATP.

As with other potexvirus, BaMV replicase contains a helicase-like domain which can be classified into SF1. In this study, contributions of the conserved motifs of the helicase-like domain to NTPase and RNA 5′-triphosphatase were investigated by mutagenesis. With respect to ATPase activity, motifs I and II are essential, consistent with the suggestions by crystal structures and mutational results reported in numerous literatures. Mutations at the aspartate of motif III and the arginine of motif VI brought on severe damages to the activity, also consistent with their involvement in ATP binding. Function of DEIH sequence immediately downstream motif VI is not

Fig. 9. Local lesions on *C. quinoa* leaves at the 18th day post inoculation. Inoculation of *C. quinoa* leaves with various pCBG clones was as described under Materials and methods. Mock was done with water.

analogous to that of DEXH box (motif II) of SF2 helicases because mutation of the sequence merely caused about 10-fold decrease in k_{cat} value. Q826 in motif V seems to avoid the tight binding of the protein to ground-state ATP since alanine substitution at the residue reduced value of $K_{m(ATP)}$ notably. The otherwise enhanced affinity to ATP in Q826A not only had adverse effect on ATP hydrolysis but also caused significant interference with RNA 5′-triphosphatase activity. L543, located in a predicted short β-strand outside the helicase motifs, might have a structural role supporting the active-site architecture for catalyzing ATP hydrolysis. For one thing, L543 bears a hydrophobic side chain; for another, the destructive effect caused by proline substitution could be reversed to a certain extent by alanine substitution. Nonetheless, this proposition needs to be verified by further structural analysis. As for RNA 5′-triphosphatase activity, the effects caused by the various mutations were similar to those on ATPase activity, except for Q826A: the alanine substitution increased $K_{m(RNA)}$ slightly for the RNA 5′-triphosphatase activity, while decreasing $K_{m(ATP)}$ for the NTPase activity more than 17-fold. The importance of the mutated residues in the viral accumulation in plant was also investigated. Mutations of residues within the conserved motifs would disable the viral replication *in vivo*. By contrast, the two mutations outside the motifs, L543A and D858A, had insignificant consequence. The helicase motifs in 1a protein of brome mosaic virus have also been shown to play essential roles in RNA replication *in vivo* by presumably being involved in viral RNAs import (Wang et al., 2005).

Another aim of this study is to know whether the two enzymatic activities occur at a single or two independent catalytic sites. The generally parallel effects of the mutations on the two activities suggest that the protein employs the same amino acid constellation for the removal of 5′ γ-phosphate from RNA and NTP. Approximation between $K_{i(AMPPNP)}$ in RNA 5′-triphosphatase competition assays and $K_{m(ATP)}$ in ATPase assays supports the same idea. Still, we cannot rule out another possibility that the substrates might bind to two closely related sites with the ATPase activity driving a conformational change that activates the RNA 5′-triphosphatase activity, considering the opposite mutational effects on $K_{m(ATP)}$ and $K_{m(RNA)}$ of Q826A. Further structural evidence is needed to clarify the argument. Nonetheless, employment of a common catalytic site for NTPase and RNA 5′-triphosphatase activities has also been suggested on several helicase motif-base proteins such as SFV nsp2 (Balistreri et al., 2007), reovirus λ1 (Bisaillon and Lemay, 1997), SARS-coronavirus nsp13 (Ivanov et al., 2004) and dengue virus nsp3 proteins (Bartelma and Padmanabhan, 2002). This raises a question as whether RNA 5′-triphosphatase activity is an attendant function of helicases, or it is an adaptive outcome in the course of viral evolution. BaMV genome contains two copies of helicase-like domains. One is the domain within viral replicase, the other is the P28 movement protein encoded by triple gene block. With the essential role to the movement of virus in the infected plant, P28 protein also possesses NTPase and RNA-binding activities (Wung et al., 1999); however, it did not show RNA 5′-triphosphatase activity (Li et al., 2001b). Taken together with the fact that only a few helicases (or helicase-like proteins) have been reported to have RNA 5′-triphosphatase activity, we speculate that the 5′ γ-phosphohydrolase activity for RNA molecule has evolved from NTPase activity driven by the demand for functional capping machinery, by which the mRNA of RNA viruses can be capped within cytoplasm of the infected cells.

In spite of lacking explicit biochemical data, the helicase-like domain of BaMV replicase has been thought to have RNA helicase activity, which may be required for resolving intramolecular base pairing in the template RNA and/or preventing the formation of extensive base pairing between template and the nascent complementary strand during RNA replication process. Is it possible that a protein domain can participate in RNA replication while it is also responsible for the removal of 5′ γ-phosphate from the nascent RNA to allow cap structure formation? With the help of the flanking flexible hinges, the helicase-like domain may be able to work with the RdRp or the capping domains at different steps during replication process. Yet, we cannot rule out another possibility at this moment that the function of the helicase-like domain is for the formation of cap structure while the helicase activity required for BaMV replication is provided by hosts. Deferring the uncertainty of helicase activity, RNA 5′-triphosphatase itself is definitely sufficient to dictate the survival of BaMV in plant. Mutations that abolished the enzymatic activity in vitro could result in the demise of the virus in *C. quinoa*. Nonetheless, ~7% of the wild-type activity, in terms of k_{cat}/K_m, seemed to be enough for the need since BaMV bearing D858A mutation survived. The failure of Q826A mutant in *C. quinoa* is intriguing because it has even higher RNA 5′-triphosphatase function than D858A. Further inhibition of the weaken RNA 5′-triphosphatase activity by tight binding of ATP *in vivo* might account for the fatal outcome, indicating the need of a multiple-function enzyme to coordinate all its activities for the survival of the organism.

Materials and methods

Plasmids and site-directed mutagenesis

Plasmid pHWT, a pET32 derived-vector containing a cDNA fragment encoding amino acids 514–892 of BaMV replicase, was used for protein expression in *E. coli* as described previously (Li et al., 2001b). Plasmid pCBG is an infectious clone of recombinant BaMV, in which a green fluorescence protein (GFP) gene preceded by a duplicated coat protein promoter is situated between triple gene block and coat protein-coding region as described previously (Lin et al., 2004). Initial transcription of the recombinant BaMV genome from pCBG in plant is driven by 35S promoter of cauliflower mosaic virus. Plasmid pUHel is a pUC18-based vector that contains an *Sph*I-digested fragment (4168 nt) isolated from pCBG. Site-directed mutagenesis was done on pHWT and pUHel based on the protocol of QuikChange site-directed mutagenesis kit (Stratagene). After confirming the mutations with ABI Prism 3100 auto sequencer (PerkinElmer), the *Sph*I-digested fragment from the mutated pUHel was put back into pCBG.

Protein expression and purification

The helicase-like domain of BaMV replicase, fused with a thioredoxin, a poly-histidine tag, and an S-tag at the N terminus, was expressed in *E. coli* Novablue cells (Novagen) and purified as described previously with minor modifications (Li et al., 2001b). Briefly, the recombinant protein, expressed as inclusion bodies, was first dissolved in urea-containing lysis buffer (50 mM Tris [pH 7.5], 150 mM KCl, 0.1% Brij-35, 10% glycerol, 10 mM β-mercaptoethanol, 1 mM PMSF and 8 M urea). Refolding of the protein was done at 4 °C by dropping 1 ml denatured protein solution (~15 mg/ml) into 25 ml stirred lysis buffer. After centrifugation, the refolded protein in the supernatant was then purified by Ni^{2+}-nitriloacetic acid resin (Qiagen) followed by Q Sepharose (Pharmacia) using a linear gradient of NaCl (20–500 mM) in equilibrium buffer (50 mM Tris [pH 8.0], 0.1% Brij-35, 20% glycerol, 10 mM β-mercaptoethanol, and 5 mM EGTA). The eluted protein was finally subjected to dialysis against equilibrium buffer containing additional 20 mM KCl.

RNA preparation

RNA transcript consisting of the first 50 nucleotides of the plus-strand RNA of BaMV was used as substrate for RNA 5′-triphosphatase assay. The corresponding cDNA fragment preceded by T7 promoter was first amplified from a cDNA clone of BaMV by PCR and purified through steps of PAGE (10%), gel extraction and ethanol precipitation. The amplified cDNA fragment was then used as template to produce 5′-[γ-^{32}P]RNA in a 20-μl *in vitro* transcription reaction that contained 0.3 μg template DNA, 30 mM NTP (7.5 mM each), 0.05 mCi [γ-^{32}P]GTP (6000 Ci/mmol, PerkinElmer), 2 μl T7-MEGAshortscript enzyme mix (Ambion) and 1× T7 transcription buffer. After 2 h of incubation at 37 °C, the reaction product was treated with 2 units of RNase-free DNase I (Ambion) at 37 °C for 15 min and the 5′-labeled RNA was purified through 8 M urea–PAGE (10%), gel extraction and ethanol precipitation. RNA concentration was determined according to its optical density at 260 nm measured with NanoDrop spectrophotometer. A 200-nucleotide 5′-terminal fragment of the plus-strand RNA of BaMV was also prepared based on the above procedure and described before (Li et al., 2001b).

Activity assay

NTPase activity was analyzed by detecting the liberated [α-^{32}P]NDP from [α-^{32}P]NTP on a polyethyleneimine (PEI)-cellulose thin-layer chromatography (TLC) plat or by the decreasing rate of $OD_{340\ nm}$ in an enzyme-coupled assay in which NTP hydrolysis was linked to NADH oxidation through activities of pyruvate kinase and lactate dehydrogenase as described previously (Li et al., 2001b). In principle, the reactions were carried out at 20 °C in solution containing 50 mM Tris [pH 7.5], 5 mM $MgCl_2$, 5 mM DTT and indicated amounts of substrate and protein. For enzyme-coupled assays, the solution also contained 2 mM phosphoenol pyruvate, 0.2 mM NADH, 20 U of pyruvate kinase and 20 U of lactate dehydrogenase unless otherwise indicated.

RNA 5′-triphosphatase activity was analyzed by measuring the γ-phosphate released from 5′-[γ-^{32}P]RNA on PEI TLC plate using a phosphorimager (Typhoon 9200). Standard reaction was performed at 20 °C in solution containing 50 mM Tris [pH 7.5], 5 mM $MgCl_2$, 5 mM DTT, 5 U of RNase inhibitor (Takara) and specified amounts of protein and 5′-[γ-^{32}P]RNA. Reaction was stopped by adding EDTA to final 25 mM. TLC was developed using 0.15 M LiCl–0.15 M formic acid. Inhibition experiments of RNA 5′-triphosphatase were conducted in the presence of indicated amounts of ATP, AMPPNP, or AMP. The amount of radiolabeled products on TLC plate was quantified according to its pixel count against a standard curve of serial diluted 5′-[γ-^{32}P]RNA versus their respective pixels. The reaction rate was estimated from a period of reaction during which no more than 15% of the initial RNA substrate was hydrolyzed. Proportional ratio between the product released and the enzyme applied under this criterion (Fig. 4B) suggests that the rates estimated should be close to the initial rate.

The Mechaelis–Menten constant, K_m and V_{max} were determined from Lineweaver–Burk plot using Grafit software. Inhibition of AMPPNP was assessed using Lineweaver–Burk plot in the presence of different fixed concentrations of AMPPNP. The inhibition constant, K_i, was calculated according to the dependence of the slope, K_m/V_{max}, of the Lineweaver–Burk plot on the inhibitor concentration. Catalytic constant, k_{cat}, was calculated based on the equation $V_{max}=k_{cat}\times[E]_0$ where $[E]_0$ is the molar concentration of the protein used in assays.

Multiplication of recombinant BaMV in leaves of C. quinoa

Plasmid pCBG and its derivatives were inoculated mechanically into plant leaves of 3-week-old *C. quinoa* according to the method described previously with minor modifications (Lin and Hsu, 1994). In short, 2 μg DNA in 10 μl aqueous solution was rubbed gently over the surface of the selected leaf that had been dusted with a thin layer of sterile carborundum. Each plasmid DNA was applied to at least 9 leaves, 3–4 leaves a plantlet and total 3 plantlets. Fluorescent images of inoculated leaves were obtained 7 days post-inoculation with a FluorImager with an excitation filter of 488 nm and an emission filter using calibration files. Spots with green fluorescence were further observed under a fluorescent microscope. Local lesions that appeared later on leaves could be observed by naked eyes.

Acknowledgments

This work was supported by grants, NSC 94-2752-B-005-012-PAE, from the National Science Council, Taiwan, Republic of China.

References

Ahola, T., Ahlquist, P., 1999. Putative RNA capping activities encoded by brome mosaic virus: methylation and covalent binding of guanylate by replicase protein 1a. J. Virol. 73, 10061–10069.

Ahola, T., Kääriäinen, L., 1995. Reaction in alphavirus mRNA capping: formation of a covalent complex of nonstructural protein nsP1 with 7-methyl-GMP. Proc. Natl. Acad. Sci. U.S.A. 92, 507–511.

Balistreri, G., Caldentey, J., Kääriäinen, L., Ahola, T., 2007. Enzymatic defects of the nsP2 proteins of Semliki Forest virus temperature-sensitive mutants. J. Virol. 81, 2849–2860.

Bartelma, G., Padmanabhan, R., 2002. Expression, purification, and characterization of the RNA 5′-triphosphatase activity of dengue virus type 2 nonstructural protein 3. Virology 299, 122–132.

Bisaillon, M., Lemay, G., 1997. Characterization of the reovirus λ1 protein RNA 5′-triphosphatase activity. J. Biol. Chem. 272, 29954–29957.

Bisaillon, M., Bergeron, J., Lemay, G., 1997. Characterization of the nucleoside triphosphate phosphohydrolase and helicase activities of the reovirus λ1 protein. J. Biol. Chem. 272, 18298–18303.

Changela, A., Ho, C.K., Martins, A., Shuman, S., Mondragon, A., 2001. Structure and mechanism of the RNA triphosphatase component of mammalian mRNA capping enzyme. EMBO J. 20, 2575–2586.

Gomez de Cedron, M., Ehsani, N., Mikkola, M.L., Garcia, J.A., Kääriäinen, L., 1999. RNA helicase of Semliki Forest virus replicase protein NSP2. FEBS Lett. 448, 19–22.

Goregaoker, S.P., Culver, J.N., 2003. Oligomerization and activity of the helicase domain of the tobacco mosaic virus 126- and 183-kilodalton replicase proteins. J. Virol. 77, 3549–3556.

Hampp, R., Goller, M., Ziegler, H., 1982. Adenylate Levels, energy charge, and phosphorylation potential during dark–light and light–dark transition in chloroplasts, mitochondria, and cytosol of mesophyll protoplasts from *Avena sativa* L. Plant Physiol. 69, 448–455.

Ho, C.K., Pei, Y., Shuman, S., 1998. Yeast and viral RNA 5′ triphosphatases comprise a new nucleoside triphosphatase family. J. Biol. Chem. 273, 34151–34156.

Huang, C.-Y., Tsai, C.-H., 1998. Evolution of bamboo mosaic virus in a nonsystemic host results in mutations in the helicase-like domain that cause reduced RNA accumulation. Virus Res. 58, 127–136.

Huang, C.-Y., Huang, Y.-L., Meng, M., Hsu, Y.-H., Tsai, C.-H., 2001. Sequences at the 3′ untranslated region of bamboo mosaic potexvirus RNA interact with the viral RNA-dependent RNA polymerase. J. Virol. 75, 2818–2824.

Huang, Y.-L., Hsu, Y.-H., Han, Y.-T., Meng, M., 2005. mRNA guanylation catalyzed by the *S*-adenosylmethionine-dependent guanylyltransferase of bamboo mosaic virus. J. Biol. Chem. 280, 13153–13162.

Ivanov, K.A., Ziebuhr, J., 2004. Human coronavirus 229e nonstructural protein 13: characterization of duplex-unwinding, nucleoside triphosphatase, and RNA 5′-triphosphatase activities. J. Virol. 78, 7833–7838.

Ivanov, K.A., Thiel, V., Dobbe, J.C., van der Meer, Y., Snijder, E.J., Ziebuhr, J., 2004. Multiple enzymatic activities associated with severe acute respiratory syndrome coronavirus helicase. J. Virol. 78, 5619–5632.

Kadaré, G., Haenni, A.L., 1997. Virus-encoded RNA helicases. J. Virol. 71, 2583–2590.

Kong, F., Sivakumaran, K., Kao, C., 1999. The N-terminal half of the brome mosaic virus 1a protein has RNA capping-associated activities: specificity for GTP and S-adenosylmethionine. Virology 259, 200–210.

Korolev, S., Hsieh, J., Gauss, G.H., Lohman, T.M., Waksman, G., 1997. Major domain swiveling revealed by the crystal structures of complexes of *E. coli* rep helicase bound to single-stranded DNA and ADP. Cell 90, 635–647.

Li, Y.-I., Cheng, Y.-M., Huang, Y.-L., Tsai, C.-H., Hsu, Y.-H., Meng, M., 1998. Identification and characterization of the *Escherichia coli*-expressed RNA-dependent RNA polymerase of bamboo mosaic virus. J. Virol. 72, 10093–10099.

Li, Y.-I., Chen, Y.-J., Hsu, Y.-H., Meng, M., 2001a. Characterization of the AdoMet-dependent guanylyltransferase activity that is associated with the N terminus of bamboo mosaic virus replicase. J. Virol. 75, 782–788.

Li, Y.-I., Shih, T.-W., Hsu, Y.-H., Han, Y.-T., Huang, Y.-L., Meng, M., 2001b. The helicase-like domain of plant potexvirus replicase participates in formation of RNA 5′ cap structure by exhibiting RNA 5′-triphosphatase activity. J. Virol. 75, 12114–12120.

Lin, N.-S., Hsu, Y.-H., 1994. A satellite RNA associated with bamboo mosaic potexvirus. Virology 202, 707–714.

Lin, N.-S., Lin, B.-Y., Lo, N.-W., Hu, C.-C., Chow, T.-Y., Hsu, Y.-H., 1994. Nucleotide sequence of the genomic RNA of bamboo mosaic potexvirus. J. Gen. Virol. 75, 2513–2518.

Lin, M.-K., Chang, B.-Y., Liao, J.-T., Lin, N.-S., Hsu, Y.-H., 2004. Arg-16 and Arg-21 in the N-terminal region of the triple-gene-block protein 1 of bamboo mosaic virus are essential for virus movement. J. Gen. Viol. 85, 251–259.

Magden, J., Takeda, N., Li, T., Auvinen, P., Ahola, T., Miyamura, T., Merits, A., Kääriäinen, L., 2001. Virus-specific mRNA capping enzyme encoded by hepatitis E virus. J. Virol. 75, 6249–6255.

Martins, A., Shuman, S., 2003. Mapping the triphosphatase active site of baculovirus mRNA capping enzyme LEF4 and evidence for a two-metal mechanism. Nucleic Acids Res. 31, 1455–1463.

Matusan, A.-E., Pryor, M.-J., Davidson, A.-D., Wright, P.-J., 2001. Mutagenesis of the dengue virus type 2 NS3 protein within and outside helicase motifs: effects on enzyme activity and virus replication. J. Virol. 75, 9633–9643.

Merits, A., Kettunen, R., Makinen, K., Lampio, A., Auvinen, P., Kääriäinen, L., Ahola, T., 1999. Virus-specific capping of tobacco mosaic virus RNA: methylation of GTP prior to formation of covalent complex p126-m7GTP. FEBS Lett. 455, 45–48.

Subramanya, H.S., Bird, L.E., Brannigan, J.A., Wigley, D.-B., 1996. Crystal structure of a DExx box DNA helicase. Nature 384, 379–383.

Suzich, J.-A., Tamura, J.-K., Palmer-Hill, F., Warrener, P., Grakoui, A., Rice, C.M., Feinstone, S.M., Collett, M.S., 1993. Hepatitis C virus NS3 protein polynucleotide-stimulated nucleoside triphosphatase and comparison with the related pestivirus and flavivirus enzymes. J. Virol. 67, 6152–6158.

Takagi, T., Moore, C.R., Diehn, F., Buratowski, S., 1997. An RNA 5′-triphosphatase related to the protein tyrosine phosphatases. Cell 89, 867–873.

Tamura, J.K., Warrener, P., Collett, M.S., 1993. RNA-stimulated NTPase activity associated with the p80 protein of the pestivirus bovine viral diarrhea virus. Virology 193, 1–10.

Usuda, H., 1988. Adenine nucleotide levels, the redox state of the NADP system, and assimilatory force in nonaqueously purified mesophyll chloroplasts from maize leaves under different light intensities. Plant Physiol. 88, 1461–1468.

Vasiljeva, L., Merits, A., Auvinen, P., Kääriäinen, L., 2000. Identification of a novel function of the alphavirus capping apparatus: RNA 5′-triphosphatase activity of Nsp2. J. Biol. Chem. 275, 17281–17287.

Velankar, S.S., Soultanas, P., Dillingham, M.S., Subramanya, H.S., Wigley, D.B., 1999. Crystal structures of complexes of PcrA DNA helicase with a DNA substrate indicate an inchworm mechanism. Cell 97, 75–84.

Wang, X., Lee, W.-M., Watanabe, T., Schwartz, M., Janda, M., Ahlquist, P., 2005. Brome mosaic virus 1a nucleoside triphosphatase/helicase domain plays crucial roles in recruiting RNA replication templates. J. Virol. 79, 13747–13758.

Warrener, P., Tamura, J.K., Collett, M.S., 1993. RNA-stimulated NTPase activity associated with yellow fever virus NS3 protein expressed in bacteria. J. Virol. 67, 989–996.

Wung, C.-H., Hsu, Y.-H., Liou, D.-Y., Huang, W.-C., Lin, N.-S., Chang, B.-Y., 1999. Identification of the RNA-binding sites of the 28 kDa movement protein of bamboo mosaic potexvirus. J. Gen. Virol. 80, 1119–1126.

Yao, N., Hesson, T., Cable, M., Hong, Z., Kwong, A.D., Le, H.V., Weber, P.C., 1997. Structure of the hepatitis C virus RNA helicase domain. Nat. Struct. Biol. 4, 463–467.